American Mineralogist, Volume 82, pages 368–378, 1997

Degassing of alkalic basalts

JACQUELINE EABY DIXON

Division of Marine Geology and Geophysics, Rosenstiel School of Marine and Atmospheric Science, University of Miami, 4600 Rickenbacker Causeway, Miami, Florida 33149, U.S.A.

ABSTRACT

In order to model quantitatively exsolution of volatiles over the range of basaltic melt compositions found on oceanic islands, I present compositional parameterizations of H_2O and CO_2 solubilities and use these parameterizations to develop vapor saturation and degassing models for alkalic basaltic liquids. Vapor-saturation diagrams generated as a function of melt composition are used to determine the pressure at which the melt was last in equilibrium with a vapor and the composition of the vapor phase based on measured H_2O and CO_2 contents in basaltic glasses. These models allow the calculation of the pressure at which a magma of known initial volatile content reaches vapor saturation and begins to exsolve a vapor phase. The higher solubility of CO_2 in alkalic magmas causes vapor saturation in CO_2-bearing alkalic magmas to be reached at lower pressures than in CO_2-bearing tholeiitic magmas having identical volatile contents. However, if variations in major element and volatile concentrations were linked by variations in the extent of melting, then volatile-rich, strongly alkalic magmas would begin to exsolve a vapor at slightly higher pressures than volatile-poor alkali olivine basalts or tholeiites.

Partitioning of H_2O and CO_2 into the vapor during volatile exsolution is controlled by the difference between H_2O and CO_2 solubilities. As melts become more alkalic, the relative difference between H_2O and CO_2 solubilities decreases, thus diminishing the preferential partitioning of CO_2 into the vapor. Exsolution of volatiles from tholeiites is characterized by strong partitioning of CO_2 into the vapor such that most or all CO_2 is lost before any significant loss of H_2O. In contrast, the combination of higher CO_2 solubility and higher volatile contents (and perhaps higher CO_2/H_2O ratio) in alkalic melts results in less fractionation between CO_2 and H_2O during volatile exsolution.

INTRODUCTION

Volatiles play an important role in the generation and evolution of mantle-derived melts, affecting the extent of mantle melting, liquidus phase relationships, physical properties of melts, and explosivity of volcanic eruptions. Alkalic lavas from oceanic islands provide a wealth of information on mantle heterogeneities with respect to major and trace elements and radiogenic isotopes, but heterogeneities in mantle volatiles remain poorly known. Determining heterogeneities in mantle volatiles is important to characterize mantle reservoirs fully, to understand the role of volatiles in igneous processes in different tectonic environments, and to constrain global cycling of these elements. However, to investigate the underlying mantle volatile concentrations, it is first necessary to see through the window of shallow level processes such as degassing and assimilation.

Recently, Dixon and Stolper (1995) presented a quantitative degassing model for tholeiitic basaltic melts and used this model to gain insight into exsolution of volatiles from oceanic tholeiitic magmas. This study extends their model to alkalic basaltic compositions. I present new compositional parameterizations of H_2O and CO_2 solubilities and incorporate them into mixed H_2O-CO_2 vapor saturation and degassing models for alkalic basaltic melts.

SOLUBILITY MODELS

Review of H_2O and CO_2 solubilities in tholeiitic melts

Calculation of H_2O and CO_2 solubilities in tholeiitic melts using the Stolper thermodynamic model (i.e., the activity of H_2O is taken to be the activity of molecular H_2O in the melt; Holloway and Blank 1994) involves (1) calculation of H_2O or CO_2 fugacities at the P and T of interest; (2) calculation of the mole fractions of molecular H_2O or carbonate ions in the melt in equilibrium with pure H_2O or CO_2 vapor; and (3) calculation of total H_2O or carbon dioxide concentrations in the melt. The advantage of Stolper-type solubility models for degassing calculations is that the activities of both molecular H_2O and carbonate in basaltic melt follow Henry's law at the low pressures of degassing. Also, the thermodynamic properties determined in the end-member systems can be used to calculate saturation concentrations of H_2O and CO_2 in mixed volatile systems.

Fugacities are calculated using a modified Redlich-Kwong (MRK) equation of state (Holloway 1977). At the

0003–004X/97/0304–0368$05.00

high T (~1200 °C) and low P (<4 kbar) relevant to degassing of basaltic melts, differences between fugacities calculated using various equations of state, including even the ideal gas law, are not significant. If this model were to be used at pressures greater than ~4 kbar, however, the Saxena and Fei (1987) equation of state should be used to calculate fugacities, particularly for CO_2 (Holloway and Blank 1994).

The amounts of carbonate and molecular H_2O dissolved in tholeiitic melts coexisting with pure carbon dioxide or H_2O vapor at 1200 °C can be calculated from the following equations (Dixon et al. 1995):

$$X^{m}_{CO_3^{2-}}(P, T_0) = X^{m}_{CO_3^{2-}}(P_0, T_0)\frac{f_{CO_2}(P, T_0)}{f_{CO_2}(P_0, T_0)} \cdot \exp\left\{\frac{-\Delta V_r^{o,m}(P - P_0)}{RT_0}\right\} \quad (1)$$

and

$$X^{m}_{H_2O,mol}(P, T_0) = X^{m}_{H_2O,mol}(P_0, T_0)\frac{f_{H_2O}(P, T_0)}{f_{H_2O}(P_0, T_0)} \cdot \exp\left\{\frac{(-V^{o,m}_{H_2O})(P - P_0)}{RT_0}\right\} \quad (2)$$

where X_i^m (P,T_0) is the mole fraction of carbonate or molecular H_2O in melt saturated with vapor with a fugacity of carbon dioxide or H_2O of $f_i(P,T_0)$ at pressure, P, and temperature, T_0 (1473.15 K); X_i^m (P_0,T_0) is the mole fraction of carbonate or molecular H_2O in melt in equilibrium with vapor with a fugacity of carbon dioxide or H_2O of $f_i(P_0,T_0)$ at P_0 (1 bar) and T_0; $f_{CO_2}(P_0,T_0)$ and $f_{H20}(P_0,T_0)$ = 1 bar; $X^m_{CO_3^{2-}}$ (P_0,T_0) = 3.8×10^{-7}; $X^m_{H_2O,mol}$ (P_0,T_0) = 3.28×10^{-5}; $V^{o,m}_{H_2O}$ is the molar volume of H_2O the melt in its standard state and is assumed to be constant and equal to the partial molar volume of H_2O in the melt (12 cm³/mol; Dixon et al. 1995); $\Delta V_r^{o,m} = (V^{o,m}_{CO_3^{2-}}) - (V^{o,m}_{O^{2-}})$ and $(V^{o,m}_{CO_3^{2-}})$ and $(V^{o,m}_{O^{2-}})$ are the molar volumes of the melt species in their standard states and have been taken to be independent of P and T in deriving equation (1) (23 cm³/mole; Pan et al. 1991); and R is the gas constant (83.15 cm³bar/mol·K).

Concentration of CO_2 (ppm) is calculated from mole fraction of carbonate in the melt using:

$$CO_2 \text{ (ppm)} = 10^4[4400X^m_{CO_3^{2-}}/(36.6 - 44X^m_{CO_3^{2-}})] \quad (3)$$

where 36.6 is the molecular weight for anhydrous tholeiitic basalt on a single-O basis. Calculation of H_2O concentration based on mole fraction of molecular H_2O involves three steps. First, the mole fraction of hydroxyl groups (X^m_{OH}) must be calculated as a function of the mole fraction of molecular H_2O using a regular solution model (Silver and Stolper 1989):

$$-\ln\left(\frac{(X^m_{OH})^2}{(X^m_{H_2O,mol})(1 - X^m_{H_2O,mol})}\right) = A' + B'X^m_{OH} + CX^m_{H_2O,mol} \quad (4)$$

where $A' = 0.403$, $B' = 15.333$, and $C' = 10.894$. Second, the mole fraction of total H_2O dissolved in the melt (X_B) must be calculated from the mole fractions of the individual H_2O species using:

$$X_B = X^m_{H_2O,mol} + X^m_{OH}/2. \quad (5)$$

Finally, the concentration of total H_2O dissolved in the melt (wt%H_2O_{tot}) is calculated from the total number of moles of H_2O using:

$$\text{wt\%}H_2O_{tot} = 1801.5X_B/(36.6 - 18.6X_B). \quad (6)$$

This method of determining H_2O solubility assumes a single regular solution model for H_2O speciation is valid over the conditions of glass formation. Determination of the T dependence (and consequently quench rate dependence) of H_2O speciation in silicate glasses is currently an area of active research (McMillan 1994). The quench rate dependence of H_2O speciation is not considered a significant source of error in this study because (1) no difference is detected in H_2O speciation in experimentally quenched basaltic glasses produced by quench rates differing by two orders of magnitude (Dixon et al. 1995) and (2) H_2O speciation in most oceanic basaltic glasses is within errors of the predicted speciation curve (Dixon et al. 1995; Dixon et al. 1997).

Compositional dependence of H_2O and CO_2 solubility in alkalic basaltic melts

CO_2 solubility depends strongly on melt composition though the details of this compositional dependence are poorly known (Blank and Brooker 1994; Holloway and Blank 1994). CO_2 solubility in mafic liquids recently has been determined as a function of P and T for tholeiitic (Pan et al. 1991; Dixon et al. 1995), basanitic (Holloway and Blank 1994), and leucititic (Thibault and Holloway 1994) compositions (Fig. 1). Compositions of these liquids are listed in Table 1. The CO_2 contents for these solubility studies were measured by infrared spectroscopy or a combination of bulk carbon analysis (LECO™ carbon analysis) and infrared spectroscopy, thereby minimizing discrepancies between different analytical techniques (Blank and Brooker 1994).

The temperature dependence of CO_2 solubility is also a function of melt composition, with negligible temperature dependence for tholeiitic melts (Pan et al. 1991) and strong negative temperature dependence for leucititic melts (Thibault and Holloway 1994). For example, at 10 kbar the CO_2 solubility in leucititic melt decreases from about 5 wt% at 1300 °C to about 3.2 wt% at 1600 °C (Holloway and Blank 1994). For the model presented here, T is assumed to be constant at 1200 °C, representing slightly to moderately fractionated liquids erupting on the Earth's surface.

The main purpose of this study is to provide a framework for modeling the exsolution of volatiles from alkali olivine basaltic through nephelinitic liquids erupted in submarine environments. Therefore, a compositional parameterization of CO_2 solubility over this compositional

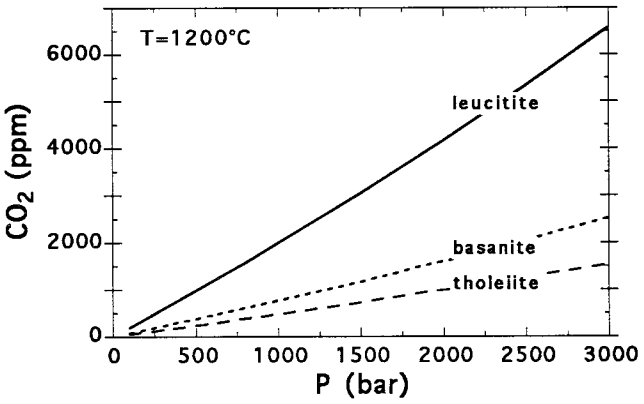

FIGURE 1. Solubility of CO_2 in mafic melts at 1200 °C using the parameters and compositions given in Holloway and Blank (1994) for tholeiite (Dixon et al. 1995), basanite (Pan and Holloway unpublished data), and leucitite (Thibault and Holloway 1994). CO_2 fugacities are calculated using an MRK equation of state (Holloway 1981, 1987).

range is required. Previous work has shown that CO_2 solubility increases as melt depolymerization increases, e.g., decreasing SiO_2 and Al_2O_3 contents or increasing proportion of non-bridging O atoms to tetrahedral cations (NBO/T) (Eitel and Weyl 1932; Mysen et al. 1976; Mysen 1976; Spera and Bergman 1980). For a given SiO_2 content, CO_2 solubility varies as a function of the proportions of metal cations (Holloway et al. 1976; Spera and Bergman 1980). Gibbs free energies of carbonation reactions (ΔG_r, Spera and Bergman 1980) suggest that the order of increasing ability of a cation to increase CO_2 solubility is $Ca^{+2} > K^{+1} > Na^{+1} \gg Mg^{+2} \approx Fe^{+2}$. Thus the compositional dependence of CO_2 solubility in mafic liquids should be able to be parameterized with two terms representing (1) melt depolymerization and (2) potential of cations to react with carbonate. I have derived an empirical relation reflecting this dependence. The first term is just the sum of the molar proportions of Si^{+4} and Al^{+3}. The second term sums the molar proportions of cations ($Ca^{+2} + 0.8K^{+1} + 0.7Na^{+1} + 0.4Mg^{+2} + 0.4Fe^{+2}$), where the coefficient for each cation is calculated from the magnitude of the Gibbs free energy of the carbonation reaction (Spera and Bergman 1980) for each cation relative to Ca^{+2} ($\Delta G_r^{Ca}/\Delta G_r^{i}$).

These two terms are combined into a compositional parameter (Π). Linearity between Π and CO_2 solubility in tholeiitic (no. 1 and no. 2), basanitic (no. 3), and leucititic (no. 4) compositions was achieved by multiple regression of $aA + bB = C = \Pi \times 10^3$, where $A = (Si^{+4} + Al^{+3})$, $B = (Ca^{+2} + 0.8K^{+1} + 0.7Na^{+1} + 0.4Mg^{+2} + 0.4Fe^{+2})$, and C = CO_2 solubility at 1 kbar and 1200 °C. Coefficients a and b were determined to be −6.50 and 20.17, respectively. Thus, the best fit value determined for Π is:

$$\Pi = -6.50(Si^{+4} + Al^{+3}) + 20.17(Ca^{+2} + 0.8K^{+1} + 0.7Na^{+1} + 0.4Mg^{+2} + 0.4Fe^{+2}). \quad (7)$$

Figure 2a shows the best-fit correlation between CO_2 solubility and P at 1 kbar and 1200 °C ($r^2 = 0.984$, standard error in predicting CO_2 solubility = 122 ppm). Under these *P-T* conditions, the CO_2 solubility increases ~4–5× from tholeiitic (Π = 0.4) to leucititic (Π = 2.2) compo-

TABLE 1. Major element compositions of glasses used in compositional parameterization of CO_2 solubility

	MORB Thol (1)	Kilauea Thol (2)	Basanite (3)	Leucitite (4)	Sodalite (5)
Oxide (wt%)					
SiO_2	49.1	49.2	46.0	44.1	46.5
Al_2O_3	16.4	13.3	15.2	12.8	19.7
Fe_2O_3	n.r.	1.72	n.r.	2.69	0.0
FeO	8.86*	9.68	12.0*	6.62	0.0
MgO	10.2	10.4	9.06	9.14	0.0
CaO	11.7	10.9	8.22	14.3	21.7
Na_2O	2.13	2.15	4.33	3.20	12.0
K_2O	0.07	0.51	1.32	3.45	0.0
TiO_2	0.74	2.29	3.17	2.69	0.0
P_2O_5	n.r.	n.r.	0.27	0.77	0.0
Total	99.2	99.7	99.6	99.8	100.0
CO_2 solubility					
1200 °C, 1 kbar (ppm)	484	543	807	2200	n.d.
1400 °C, 20 kbar (wt%)	1.48	1.60	2.30	5.77	7.19
Cation Proportions					
Si^{+4}	0.477	0.455	0.422	0.405	0.400
Al^{+3}	0.152	0.145	0.164	0.138	0.200
Fe^{+2}	0.082*	0.075	0.078	0.051*	0
Mg^{+2}	0.093	0.144	0.124	0.125	0
Ca^{+2}	0.116	0.108	0.081	0.141	0.200
Na^{+1}	0.049	0.039	0.077	0.057	0.200
K^{+1}	0.002	0.006	0.0155	0.040	0
Π*	0.41	0.70	0.81	2.19	2.96

Notes: 1: Dixon et al. (1995). 2: Pan et al. (1992). 3: Composition from Dixon and Pan 1995. CO_2 solubility data from Holloway and Blank (1994). 4: Thibault and Holloway (1994). 5: Mattey et al. (1990). n.r. means not reported. n.d. means not determined.

* $\Pi = -6.50(Si^{+4} + Al^{+3}) + 20.17(Ca^{+2} + 0.8K^{+1} + 0.7Na^{+1} + 0.4Mg^{+2} + 0.4Fe^{+2})$.

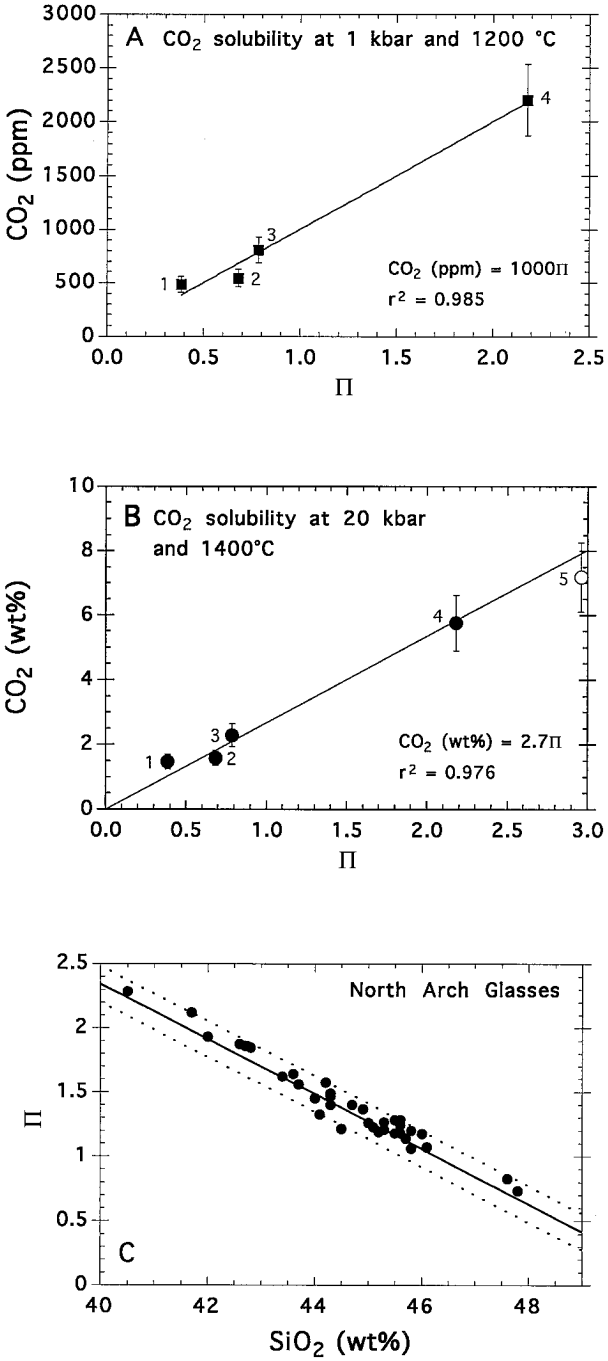

FIGURE 2. (**A**) Linear correlation between CO_2 solubility data (1 kbar and 1200 °C) and Π, an empirically derived compositional parameter (see text). Sources of data listed in caption to Table 1. Error bars for CO_2 solubility data are ±15% (relative). (**B**) CO_2 solubility data (20 kbar, 1400 °C) plotted against Π showing validity of parameterization at higher *P* and *T*. Data sources and errors are the same as (**A**). Sodamelilite (no. 5) composition was not used in the calibration to determine Π, but agrees within errors with the projected linear correlation between CO_2 solubility and Π at constant *P* and *T*. (**C**) Values of Π plotted against SiO_2 for glasses from the North Arch volcanic field (Dixon et al. 1997). Solid line is best fit line (Π = 10.9–0.214*SiO_2). Dotted lines are ± 2 standard error in calculation of Π.

→

sitions. It is important to emphasize that this compositional parameterization for CO_2 solubility at constant *P* and *T* is valid only for liquids in which carbon dissolves totally as carbonate ions and should not be used for intermediate or silicic liquids in which carbon dissolves as both carbonate ions and molecular CO_2.

Figure 2b shows the linear correlation between CO_2 solubility and Π at 20 kbar and 1400 °C. As an independent check of the calibration, the CO_2 solubility data for sodamelilite (Mattey et al. 1990) is also plotted. Although this composition was not used in the calibration, it plots within errors of the best-fit line of CO_2 solubility vs. Π for tholeiitic, basanitic, and leucititic compositions.

Given this compositional parameterization for CO_2 solubility in mafic liquids, I can now evaluate the effect of composition on CO_2 solubility in oceanic alkalic series magmas. Glasses from the North Arch volcanic field, a suite of alkalic to strongly alkalic lavas erupted on the seafloor north of Oahu (Clague et al. 1990; Dixon et al. 1997) provide a useful example. These glasses have values of Π ranging from 0.7 to 2.3. Furthermore, values of Π vary linearly with SiO_2 in these glasses (Fig. 2c; r^2 = 0.944, twice standard error in predicting Π is 0.14), allowing SiO_2 to be used as a proxy for Π for this suite of lavas and enabling a single parameter to be used to predict the compositional dependence of both CO_2 and H_2O solubility (see below). On the basis of the 1200 °C, 1 kbar data, CO_2 solubility in a volatile exsolution model designed to encompass compositions ranging from tholeiite (49 wt% SiO_2, Π = 0.45) to nephelinite (40 wt% SiO_2, Π = 2.3) would increase from ~5×. Given the scatter in the SiO_2-Π correlation (Fig. 2c), I can infer that my prediction of CO_2 solubility is good to ~15%.

This compositional parameterization can be integrated into the thermodynamic expression for CO_2 solubility. Because the values of Π in the North Arch glasses vary linearly with SiO_2 and because no apriori information is available on the compositional dependence of $\Delta V_r^{o,m}$, I allow $X^m_{CO_3^{2-}}(P_0,T_0)$ to vary as a linear function of SiO_2 and assume that $\Delta V_r^{o,m}$ is constant. The desired 5× range of solubilities for a SiO_2 range of 40–49 wt% is produced by substituting the following expression for $X^{mm}_{CO_3^{2-}}(P_0,T_0)$ into Equation 1:

$$X^m_{CO_3^{2-}}(P_0,T_0) = 8.70 \times 10^{-6} - 1.70 \times 10^{-7}\ SiO_2 \quad (8)$$

(where SiO_2 is in wt%) followed by calculation of concentration using Equation 3. The compositional dependence of the molecular weight on a single oxygen basis of mafic melts is small (~±3%) and therefore the value for tholeiitic liquid (36.6 g/mol) is used throughout the compositional range.

In contrast to CO_2, H_2O solubility is not a strong function of composition for tholeiitic through nephelinitic

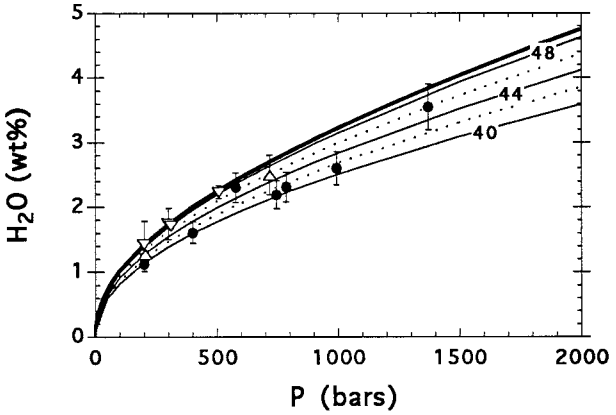

FIGURE 3. Comparison of H_2O solubilities at 1200 °C measured in tholeiitic basaltic glasses having SiO_2 of 49–50 wt% (open triangles; Dixon et al. 1995) and basanitic glasses having SiO_2 of 45 wt% (filled circles-error bars are plotted as 10% of the amount present representing ~2σ; Cocheo and Holloway 1993). Heavy curve is solubility model of Dixon et al. (1995). Light solid curves and dashed curves are H_2O solubilities as a function of SiO_2 content (labeled on curves) as presented in this study showing a 30% decrease in H_2O solubility as SiO_2 decreases from 49% (tholeiite) to 40% (nephelinite).

compositions (McMillian 1994; Holloway and Blank 1994). In consideration of a wide range of silicate melt compositions, H_2O solubility is more dependent on melt composition at low P than at high P (McMillan and Holloway 1987). However, existing models (Burnham 1994; Holloway and Blank 1994; Moore et al. 1995) predict the magnitude of the variation over the limited compositional range of tholeiitic to nephelinitic melts is small (<10% relative). These models, however, are not optimized for mafic compositions.

Recent low P experimental determinations of H_2O solubility in tholeiitic (Dixon et al. 1995) and basanitic (Cocheo and Holloway 1993) melts are directly comparable because they were determined using identical experimental and analytical techniques. Cocheo and Holloway (1993) determined that the H_2O solubility in a basanitic melt is about 20% lower than that in tholeiitic melt (Fig. 3) and that the speciation of H_2O in basanitic glass was essentially identical to that in tholeiitic glass. I have selected these results as the basis for my models because both experiments were optimized for the low pressures relevant to exsolution of volatiles from basalts and the two compositions are specifically suited to this application. For these reasons, in the models presented below I assume that H_2O solubility decreases by ~30% as melt composition changes from tholeiitic to nephelinitic and that the speciation model for tholeiitic glass (Dixon et al. 1995) is valid over the range of compositions of interest here. For completeness, the effect on the volatile exsolution models of assuming H_2O solubility to be constant over the composition range of interest will also be discussed. The important point is that the compositional dependence of H_2O solubility is small compared with that of CO_2 solubility; therefore, the compositional dependence of the volatile exsolution process is controlled dominantly by CO_2.

Analogous to the treatment of CO_2 solubility, I use a simple linear extrapolation for the compositional dependence of H_2O solubility as a function of SiO_2, content in wt%. Thus, $X^m_{H_2O,mol}(P_0,T_0)$ is allowed to vary as a linear function of SiO_2, while $V^{o,m}_{H_2O}$ is assumed to be independent of P, T, and melt composition. The appropriate range of solubilities over a SiO_2 range of 40–49 wt% are produced using the following expression for the mole fraction of molecular H_2O dissolved in the melt at standard state:

$$X^m_{H_2O,mol}(P_0, T_0) = -3.04 \times 10^{-5} + 1.29 \times 10^{-6}\ SiO_2. \quad (9)$$

Total H_2O contents are calculated from $X^m_{H_2O,mol}(P_0,T_0)$ using equations (4)–(6). The experimentally determined H_2O solubility data for basanite (SiO_2 = 45 wt%; Cocheo and Holloway 1993) agree with the predicted solubility model to better than 15% relative (Fig. 3).

VAPOR SATURATION MODELS

Evaluation of vapor saturation and calculation of H_2O-CO_2 vapor-phase composition

CO_2 and H_2O concentrations in vapor-saturated melts vary as a function of P and vapor composition. Dixon and Stolper (1995) presented a model for calculating the equilibrium pressure and vapor composition of vapor-saturated tholeiitic melts based on measured H_2O and CO_2 concentrations in the glass. An example of a vapor-saturation diagram is shown for tholeiitic melts in Figure 4a. Solid curves show the change in the amount of H_2O and CO_2 dissolved in a vapor-saturated tholeiitic melt at constant P (isobars) and 1200 °C as the vapor composition varies from pure CO_2 to pure H_2O. Dashed curves show the change in saturation values of H_2O and CO_2 as P is reduced while holding vapor composition constant (isopleths). This model provides a valuable tool for determining the pressures of vapor–melt equilibration based on measured CO_2 and H_2O concentrations of volcanic glasses. For example, a melt containing 0.9 wt% H_2O and 150 ppm CO_2 is saturated at a P of 400 bars (4 km H_2O depth) with a vapor phase having $X^v_{CO_2} = 0.8$.

To extend this type of diagram to a range in melt compositions, the equations for the compositional dependence of CO_2 and H_2O solubility must be incorporated into the equations describing vapor saturation. Vapor-saturation diagrams are constructed with the assumption that the vapor contains only CO_2 and H_2O and that the vapor mixes ideally (i.e., $f_i = X^v_i f^0_i$). If these conditions are satisfied, then the following must be true at vapor saturation:

$$\frac{a^m_{H_2O}}{a^{o,m}_{H_2O}} + \frac{a^m_{CO_3^{2-}}}{a^{o,m}_{CO_3^{2-}}} = 1 \quad (10)$$

where the a^m_i is the activity of H_2O or carbonate in the melt and $a^{o,m}_i$ is the corresponding activity in melt in equilibrium with pure H_2O or carbon dioxide. Given that the vapor mixes ideally, it can be shown that the mole frac-

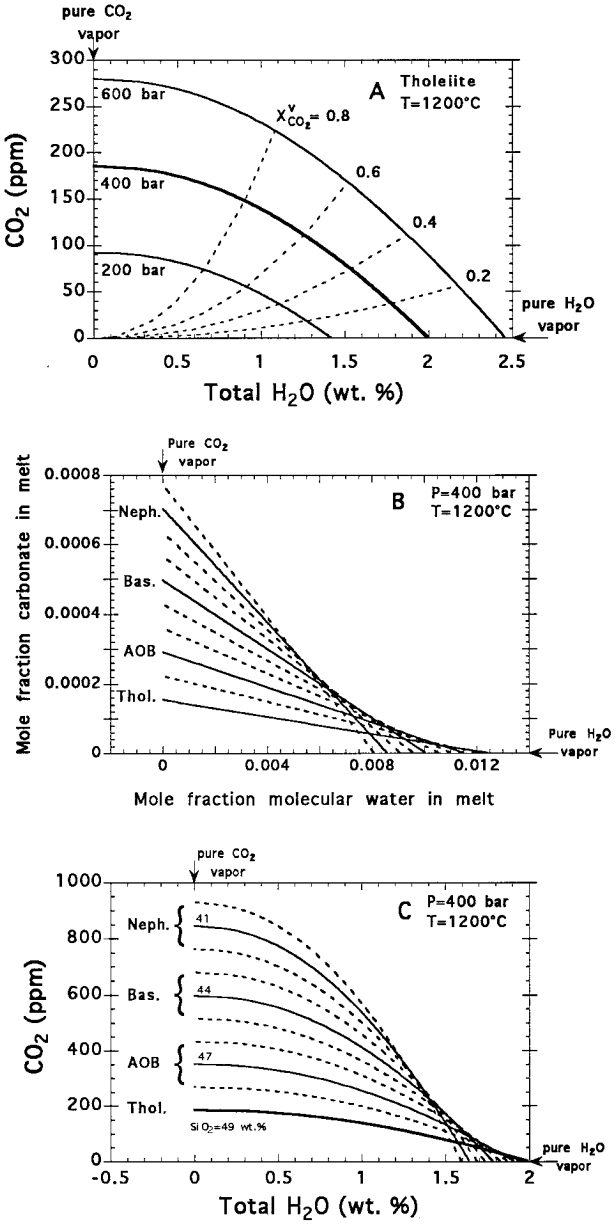

FIGURE 4. (**A**) Vapor saturation diagram for tholeiite at 1200 °C. Solid curves represent the H_2O and CO_2 contents in vapor saturated tholeiitic liquids at constant *P* (isobars) and a range in vapor compositions. Dashed curves are saturation values at constant vapor composition (isopleths) over a range in *P*. As an example at 400 bars and 1200 °C, a tholeiitic liquid in equilibrium with a vapor having 80 mol% CO_2 contains 150 ppm CO_2 and 0.9 wt% H_2O. (**B**) Compositional dependence of the inverse correlation between $X^m_{CO_3^{2-}}$ and $X^m_{H_2O,mol}$ as a function of vapor composition in vapor-saturated mafic liquids at 400 bars and 1200 °C. Solid and dashed lines are lines of constant *P* (isobars) and melt composition for nephelinitic (SiO_2 = 40 wt%) through tholeiitic (SiO_2 = 49 wt%) melts plotted at increments of 1 wt% SiO_2. Vapor compositions range from pure CO_2 along the *y*-axis to pure H_2O along the *x*-axis. (**C**) Compositional dependence of the inverse correlation between CO_2 and H_2O contents as a function of vapor composition in vapor-saturated mafic liquids at 400 bars and 1200 °C. Solid and dashed curves show the compositional dependence of vapor saturation at constant *P* (isobars) as presented in this study. The lowermost solid curve for tholeiitic liquids is identical to the 400 bars isobar in Figure 4a.
←

tions of H_2O and CO_2 in the vapor can be determined using $a^m_{H_2O}/a^{o,m}_{H_2O} = X^V_{H_2O}$ and $a^m_{CO_3^{2-}}/a^{o,m}_{CO_3^{2-}} = X^V_{CO_2}$. Dixon et al. (1995) showed that it is valid to adopt the Henrian approximations for both molecular H_2O and carbonate activities, so the activities in Equation 10 are just the mole fractions of molecular H_2O and carbonate in the melt. Equation 10 thus becomes:

$$\frac{X^m_{H_2O,mol}}{X^{o,m}_{H_2O,mol}} + \frac{X^m_{CO_3^{2-}}}{X^{o,m}_{CO_3^{2-}}} = 1 \qquad (11)$$

where X^m_i is the mole fraction of molecular H_2O or carbonate in the melt and $X^{o,m}_i$ is the corresponding mole fraction in melt in equilibrium with pure H_2O or carbon dioxide. At constant *P*, *T*, and melt composition the denominators in Equation 11 (i.e., the amounts of molecular H_2O and carbon dioxide dissolved in melts that coexist with pure H_2O vapor or carbon dioxide vapor) are constants (i.e., independent of vapor composition) and can be calculated from the equations describing solubilities and the compositional dependence for CO_2 (Eq. 1 and Eq. 8) and H_2O (Eq. 2 and Eq. 9). Thus, at constant *P*, *T*, and melt composition, Equation 11 describes a linear relationship between $X^m_{CO_3^{2-}}$ and $X^m_{H_2O,mol}$ as a function of vapor composition in vapor-saturated melts. To show the effect of melt composition on the saturation surface, isobars for $X^m_{CO_3^{2-}}$ vs. $X^m_{H_2O,mol}$ for tholeiitic through nephelinitic compositions are shown at constant *P* (400 bar) on Figure 4b.

The relationship between total dissolved H_2O and dissolved carbonate in vapor-saturated melts at a constant total *P* is nonlinear, however, because of the nonlinear relationship between the concentration of molecular H_2O and total H_2O in basalts. The compositional dependence of the 400 bar isobar for total H_2O and carbonate in tholeiitic through nephelinitic melts is shown in Figure 4c. Note the 5-fold increase in CO_2 concentration and the small decrease in H_2O concentration at saturation with pure CO_2 and H_2O, respectively. Figure 4c can be used to evaluate graphically whether a basaltic liquid (tholeiitic through nephelinitic) with known concentrations of H_2O and carbon dioxide would be vapor saturated at 1200 °C and at the *P* plotted. Alternatively, a figure comprising of a set of isobars over a range of pressures can be constructed for a single-melt composition (analogous to Fig. 4a) to evaluate the *P* at which that melt composition would be vapor saturated.

Basaltic lavas that erupted deep on the seafloor may have some of their magmatic volatiles preserved in quenched glassy rinds. As an example of the application of vapor saturation diagrams, I again use data from the North Arch volcanic field glasses (Dixon et al. 1997). The

North Arch lavas were all dredged at H_2O depths of 3900–4380 m and so are directly comparable to the 400 bar calculations summarized in Figure 4. Figure 5 compares the models given in Figure 4c to three suites of North Arch lavas, representing respectively nephelinitic (5a), basanitic (5b), and alkali olivine basaltic (5c) compositions. Good agreement exists between the measured H_2O and CO_2 contents of the North Arch glasses and the predicted vapor saturation curves. The calculated vapor-saturation indices at 400 bar for each sample [Eq. 11, where a value of 1.00 is perfect saturation (on the curve), <1.0 is undersaturated (below the curve), and >1.0 is supersaturated (above the curve)] are all within 40% of 1.0 and all but one sample are within 30% of 1.0 (mean of 1.09 ± 0.15). This agreement is within the estimated uncertainty of the model [1σ uncertainties in the H_2O analyses (~±5%), CO_2 analyses (~±20%), and compositional dependence of H_2O and CO_2 solubilities (~±15%) combine to give a total uncertainty of ~30% in the value of the saturation index] and suggests that most of the North Arch glasses were vapor saturated with a H_2O-CO_2 vapor upon quenching on the seafloor at 400 bar.

Calculation of equilibrium saturation pressure

As described above, given measurements of the H_2O and CO_2 contents of natural basaltic glasses, the *P* at which a liquid of a given composition would be vapor saturated can be determined either graphically or by substituting Equations 1 and 2 into Equation 11 and then iteratively solving for *P*. For purposes of illustration, the *P* at which an ascending melt first reaches saturation as a function of melt composition and initial volatile concentrations is shown in Figures 6a–c. Upon continued depressurization, a vapor phase begins to exsolve. Figure 6a shows the dramatic decrease in saturation *P* as the melt composition becomes more SiO_2 undersaturated (more alkalic) as a consequence of increasing CO_2 solubility. For example, a nephelinite with 2.0 wt% H_2O and 2.0 wt% CO_2 reaches saturation at ~7 kbar, whereas a tholeiite with identical volatile contents reaches saturation at ~18 kbar. Figure 6a shows the effect of changing the CO_2 content at constant H_2O. Figure 6b shows the effect of changing H_2O content at constant CO_2/H_2O. For a given melt composition, both figures show the expected trend that melts with higher volatile contents reach saturation at greater depths.

In many alkalic lava series, however, trends in trace element concentrations suggest that the lavas can be related by variable extents of melting of a homogeneous source region (Clague and Frey 1982; Clague and Dalrymple 1988). Therefore, it is probably not realistic to assume that various melt compositions in an alkalic magma series were generated with identical initial volatile contents. Though the behavior of volatiles during melting is not yet well understood, this model provides a tool for investigating the consequences of various assumptions. For example, Figure 6c shows the effect of allowing the

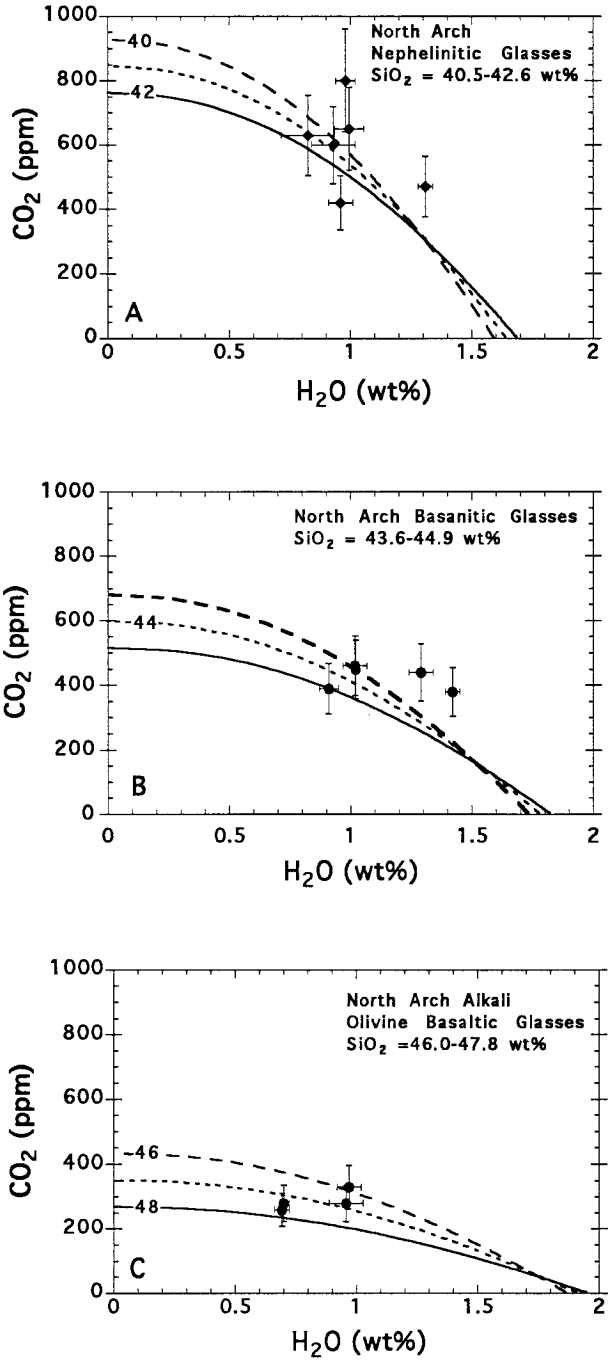

FIGURE 5. CO_2 and H_2O contents determined by FTIR in glasses from the submarine North Arch Volcanic Field erupted at 3900–4390 m H_2O depth (Clague et al. 1990; Dixon et al. 1997) plotted against the compositionally appropriate 400 bars isobars. (**A**) Nephelinitic glasses, SiO_2 = 40–42 wt%. (**B**) Basanitic glasses, SiO_2 = 43–45 wt%. (**C**) Alkali olivine basaltic glasses, SiO_2 = 46–48 wt%.

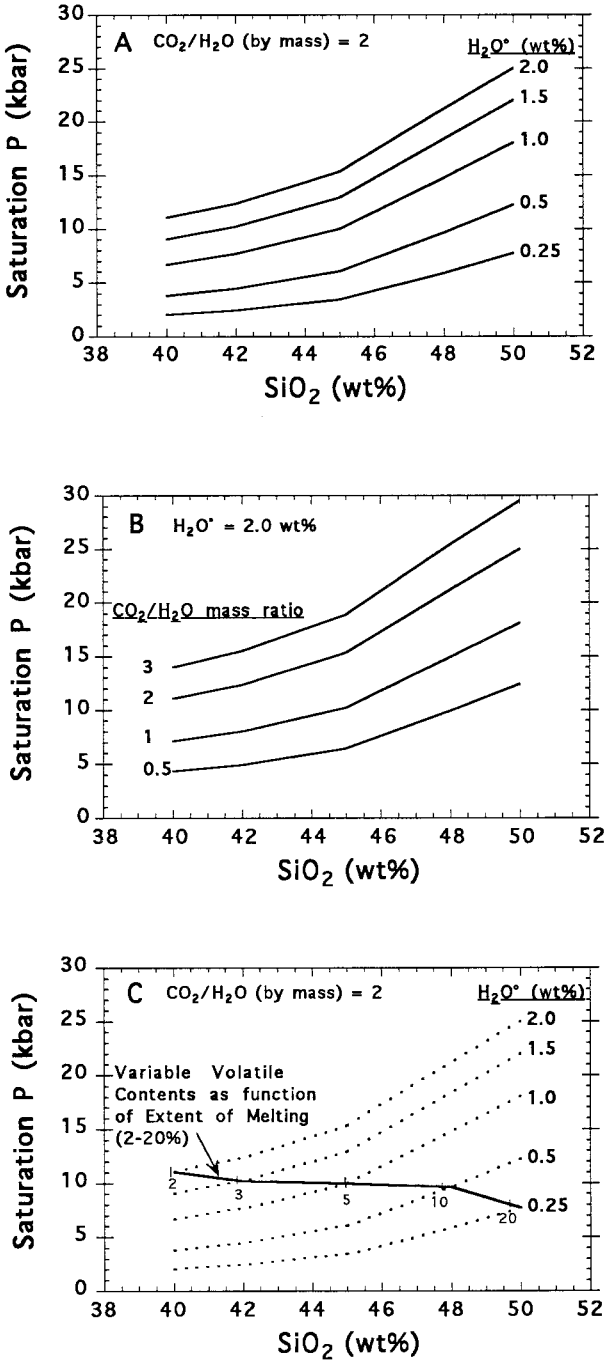

FIGURE 6. Plot of P at which an ascending magma would reach vapor-saturation as a function of initial volatile content and melt composition. (**A**) Curves of saturation P as a function of melt composition for melts having a range in initial H_2O contents at CO_2/H_2O = 2. (**B**) Curves of saturation P as a function of melt composition for melts having an initial H_2O content of 2.0 wt% and a range of CO_2/H_2O of 3–0.5. (**C**) Dashed curves are reproduced from A. Solid curve represents pressure of initial vapor saturation for mafic melts whose major element compositions and initial volatile contents are controlled by variable extents of melting. Parameters used: H_2O content in mantle source region of 600 ppm, bulk distribution content for H_2O ($D^0_{H_2O}$) of 0.010, and batch melting equation: $H_2O^m = H_2O^{source}/[D^0_{H_2O} + F(1 - D^0_{H_2O})]$. Tick marks show H_2O contents (2.0, 1.5, 1.0, 0.55, and 0.29 wt% H_2O) generated by variable extents of melting (2, 3, 5, 10, and 20%, respectively).

initial volatile concentration to vary with silicate melt composition. In this example, CO_2 and H_2O are modeled as incompatible elements, the mantle CO_2/H_2O is assumed to be constant and equal to 2 (by mass), and the extent of melting varies from 2–20%, such that a nephelinitic melt has 2.0 wt% H_2O and 40 wt% SiO_2 and a tholeiitic melt has 0.25 wt% H_2O and 50 wt% SiO_2. Using these boundary conditions, the saturation P remains nearly constant at ~8–11 kbar, and a nephelinitic melt reaches saturation at a slightly greater P than a tholeiite. The depth range over which vapor saturation is reached narrows because the relative effects of changes in CO_2 solubility and volatile contents are similar in magnitude but opposite in sign and nearly cancel. Similar trends are observed at different CO_2/H_2O ratios (for CO_2/H_2O = 1, P_{sat} = 4–7 kbar; for CO_2/H_2O = 3, P_{sat} = 10–14 kbar). Thus, in a region where the mantle is melting by variable amounts, all melts may reach saturation and begin vesiculating over a narrow range of pressures. This may have important consequences for initiation of melt segregation and transport. In addition, it suggests that the depth of vesiculation alone is not a good indicator of initial magmatic volatile contents.

Fractionation of H_2O and CO_2 between vapor and melt

Whereas absolute solubilities control H_2O and CO_2 concentrations at vapor saturation, the relative differences in solubility control partitioning of H_2O and CO_2 into the vapor phase during volatile exsolution. According to the principle of vapor-melt fractionation, often applied to the study of rare gases (Jambon et al. 1986; Zhang and Zindler 1989) and volatile exsolution from tholeiitic melts (Gerlach 1986; Bottinga and Javoy 1990; Dixon et al. 1995), a vapor-saturated melt is enriched in the most soluble component whereas the vapor is enriched in the least soluble component. Eggler (1974) was one of the first to consider the effect of basaltic melt composition on vapor fractionation of H_2O and CO_2 and applied the theory to fractionation of H_2O and CO_2 during generation of mafic melts.

This concept can be expressed in terms of a fractionation factor, analogous to the fractionation factor in stable isotopic studies. Dixon and Stolper (1995) defined the CO_2-H_2O fractionation factor (β) between vapor and melt as:

$$\beta_{CO_2-H_2O,mol} = \frac{\left(\frac{N_{CO_2}}{N_{H_2O}}\right)^{vapor}}{\left(\frac{N_{CO_3^{2-}}}{N_{H_2O,mol}}\right)^{melt}} \quad (12)$$

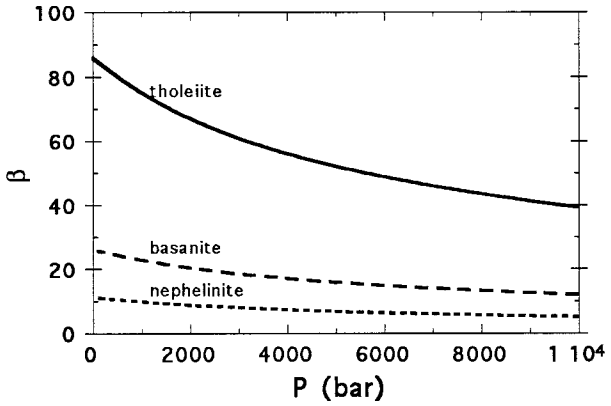

FIGURE 7. Plot of β as a function of *P* and composition for tholeiite (SiO_2 = 49 wt%), basanite (SiO_2 = 45 wt%), and nephelinite (SiO_2 = 40 wt%). Values of β calculated assuming H_2O solubility decreases with SiO_2 undersaturation according to Equation 13. The combination of increasing CO_2 solubility and decreasing H_2O solubility cause a sharp decrease in the value of β as melt composition varies from tholeiitic to nephelinitic.

where N_i is the number of moles of CO_2 and H_2O in the vapor or number of moles of carbonate and molecular H_2O in the melt. The value of β is a function of *P* and melt composition. The pressure dependence (exponential terms) of the activity of H_2O and CO_2 in tholeiitic basaltic melts at $T = 1200$ °C are given in Equations 1 and 2 and are assumed to be independent of composition. The compositional dependence of solubility is modeled by varying the standard state activities of H_2O and carbonate in the melt are given in Equations 8 and 9. Following Dixon and Stolper (1995) it can be shown that:

$$\beta_{CO_2-H_2O,mol} = \left(\frac{f^o_{H_2O}}{f^o_{CO_2}}\right)\left[\frac{\left(\frac{f_{CO_2}}{f_{H_2O}}\right)}{\left(\frac{X^m_{CO_3^{2-}}}{X^m_{H_2O,mol}}\right)}\right]$$

$$= \left(\frac{f^o_{H_2O}}{f^o_{CO_2}}\right)\left[\frac{X^{o,m}_{H_2O,mol}(1\ bar,\ 1473\ K)}{X^{o,m_2}_{CO_3^{2-}}(1\ bar,\ 1473\ K)}\right] \cdot \left(\frac{\exp\{-12(P-1)/[(83.15)(1473.15)]\}}{\exp\{-23(P-1)/[(83.15)(1473.15)]\}}\right) \quad (13)$$

Note that the fractionation factor must be expressed in terms of mole fractions of carbonate and molecular H_2O species that behave Henrian with respect to fugacities of CO_2 and H_2O in the vapor at constant *P* and *T*. The value of β is constant for a given melt composition at constant *P* and *T* (Dixon and Stolper 1995).

Values of β for tholeiitic, basanitic, and nephelinitic liquids are plotted against *P* in Figure 7. Any value of β greater than 1 indicates that CO_2 is fractionated preferentially into the vapor with respect to H_2O. The magnitude of β is related to the strength of this preferential partitioning. During depressurization and progressive exsolution of volatiles from tholeiitic melts, β is large and CO_2 is strongly partitioned into the vapor phase relative to H_2O. Thus, for a tholeiite with concentrations of H_2O and CO_2 typical of oceanic basalts, almost all CO_2 would be lost before significant quantities of H_2O begin to exsolve. Using logic based on our experience with degassing of tholeiitic melts, significant exsolution of H_2O would seem to be precluded in lavas having high CO_2 concentrations.

This logic is not valid for alkalic basalts, however, as illustrated by the strong compositional dependence of β. In general, as the melt composition changes from tholeiitic to nephelinitic, the difference between H_2O and CO_2 solubilities decreases, and the strength of fractionation of CO_2 into the vapor phase also decreases. For example, at 400 bars, the value of β ranges from 81 in tholeiitic melts (indicative of strong preferential partitioning of CO_2 into the vapor relative to H_2O) to 10 in nephelinitic melts (indicative of weak preferential partitioning of CO_2 into the vapor). Thus, if tholeiitic and nephelinitic melts with identical volatile contents degas under identical conditions, less CO_2 will degas from the nephelinitic melt than from the tholeiitic melt for a given amount of H_2O loss. Figure 7 also illustrates that β decreases with increasing *P* as a result of CO_2 fugacity increasing more rapidly with *P* than H_2O fugacity. Thus, CO_2 would not be as strongly fractionated into the vapor in melts at high pressures.

The values of β are relatively insensitive to the specific H_2O solubility model selected. The value of β for basanitic and nephelinitic liquids calculated assuming constant H_2O solubility are only slightly higher (~15–50%) than those calculated assuming that H_2O solubility decreases 30% over the tholeiitic to nephelinitic melt composition range, but this variation is small compared with the factor of 5–8 variation in β as a function of melt composition.

DEGASSING MODELS

The degassing model presented here is a modification of the one presented in Dixon and Stolper (1995). The compositional dependence of H_2O and CO_2 solubility has been incorporated in order to predict the volatile contents in alkalic magmas during depressurization and progressive volatile exsolution. [These models are the basis for interpreting the volatile exsolution history of the alkalic lavas from the North Arch volcanic field in a subsequent paper (Dixon et al. 1997)].

Degassing of tholeiitic through nephelinitic magmas can be modeled as either closed or open system. In closed system degassing, the evolved vapor stays in contact and in equilibrium with the melt throughout the entire degassing process. In open system degassing, each increment of vapor is removed immediately after exsolution resulting in accentuation of fractionation between CO_2 and H_2O (Dixon and Stolper 1995). In this paper, I focus on the closed-system case in which the effect of melt composition on degassing paths is maximized.

The models are implemented in a computer program through the following steps:

(1) Input initial H_2O and CO_2 contents, *P*, and the style of degassing (open or closed).

(2) Calculate H_2O and CO_2 solubilities and fractionation factor (β) as a function of SiO_2 content.

(3) Degas magma at a given *P* by incrementally transferring H_2O and CO_2 from the supersaturated melt into the vapor phase until saturation is reached. Each increment of volatiles partitioned into the vapor must satisfy equations for mass balance, vapor-melt fractionation, and speciation of H_2O in melt (Dixon and Stolper 1995). Saturation is evaluated using equation (11) after each increment.

(4) Output final H_2O and CO_2 contents in degassed melt, composition of vapor phase, and volume proportion vapor phase (percent vesicles).

Closed system degassing paths calculated using initial H_2O content of 2.0 wt%, CO_2 content of 1.0 wt%, and initial degassing *P* of 400 bars are shown on Figures 8a–d. The starting compositions are more volatile-rich, in particular more CO_2-rich, than the tholeiitic compositions modeled in Dixon and Stolper (1995) because alkalic basalts typically have higher total volatile contents and may be more likely to erupt in a single stage, which would limit the amount of CO_2 lost in a shallow crustal environment. For simplification, the following SiO_2 contents will be used to represent the following magma compositions-alkali olivine basalt (48% SiO_2), basanite (45% SiO_2), and nephelinite (42% SiO_2).

Figures 8a–c show that closed-system degassing of alkalic melts results in lower H_2O and higher CO_2 contents in comparison with tholeiitic melts. For example, if a nephelinite and tholeiite had degassed at 400 bars, the tholeiitic liquid would have a H_2O content of 1.5 wt% (25% loss) and a CO_2 content of 80 ppm (99.2% loss), whereas the nephelinitic liquid would have a H_2O content of 1.3 wt% (35% loss) and a CO_2 content of 340 ppm (96.6% loss). The extra H_2O loss contributes to greater proportion of H_2O in the vapor (Fig. 8d).

For completeness, additional degassing calculations were performed assuming constant H_2O solubility. In the constant H_2O solubility case, constant H_2O contents, vapor composition, and vesiculation are essentially the same for all compositions as *P* decreases (less degassing of H_2O than in the variable H_2O solubility case). CO_2 contents at a given *P* are slightly higher than in the variable H_2O solubility case for alkalic compositions, reflecting the slightly higher proportion of CO_2 in the vapor. Thus, the amount of H_2O loss during exsolution of a vapor phase is sensitive to the assumed H_2O solubility model. However, for both cases the vapor-saturated alkalic basalts have higher CO_2 contents than tholeiitic basalts degassed under identical conditions.

In summary, I have estimated the compositional dependence of H_2O and CO_2 solubility in tholeiitic through nephelinitic liquids and have generated vapor saturation and degassing models for alkalic basaltic liquids. These models provide the means to begin unraveling the exsolution of volatiles from alkalic magmas, including the pressure of last vapor saturation based on measured H_2O and CO_2 contents in glasses, the depth of initial vapor saturation based on estimates of initial H_2O and CO_2 contents, and fractionation of various volatile species during progressive depressurization. Specifically, partitioning of CO_2 into the vapor phase relative to H_2O during closed system degassing is stronger in tholeiites than in more alkalic melt compositions. During progressive exsolution of volatiles, strongly alkalic magmas will lose less CO_2 and more H_2O than tholeiitic magmas.

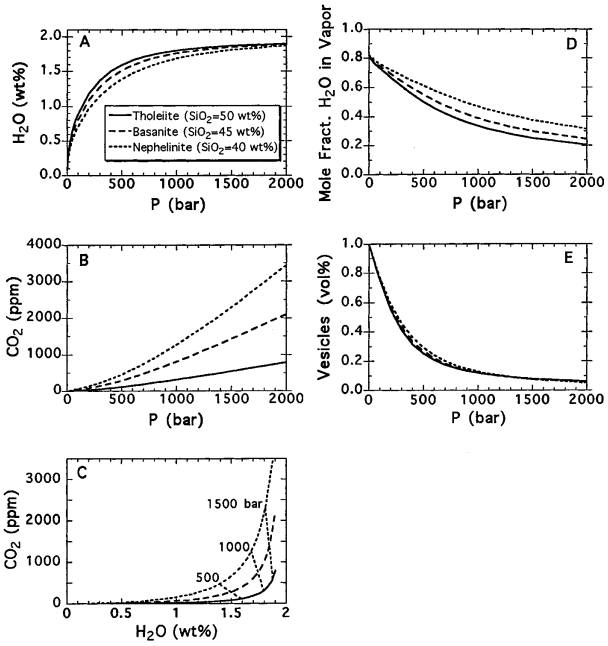

FIGURE 8. Example results of forward degassing model using the compositional dependence of CO_2 and H_2O solubility at 1200 °C on SiO_2 as presented in this study. Closed system degassing paths are shown for melts initially containing 2.0 wt% H_2O and 1.0 wt% CO_2. Results are shown for $P < 2000$ bar, though vapor saturation was reached at ~12 kbar for the tholeiite (SiO_2 = 49 wt%), ~6.5 kbar for basanite (SiO_2 = 45 wt%), and ~4 kbar for nephelinite (SiO_2 = 40 wt%). Progressive, closed system degassing was modeled as described in the text. (**A**) H_2O content as a function of *P*. (**B**) CO_2 content as a function of *P*. These values are lower than those shown in Figure 1 because the vapor contains significant amounts of H_2O. (**C**) Degassing path showing covariation of CO_2 and H_2O during progressive volatile exsolution. (**D**) Mole fraction of H_2O in vapor as a function of *P*. (**E**) Volume percent exsolved gas as a function of *P*.

ACKNOWLEDGMENTS

This work has benefited from continued interactions with David Clague, John Holloway, and Edward Stolper. Gordon Moore and Paul Wallace provided thoughtful reviews. Support was provided by NSF OCE-9302574.

References cited

Blank, J.G., and Brooker, R.A. (1994) Experimental studies of carbon dioxide in silicate melts: Solubility, speciation, and stable carbon isotope behavior. In Mineralogical Society of America Reviews in Mineralogy, 30, 157–186.

Bottinga, Y., and Javoy, M. (1990) MORB degassing: Bubble growth and ascent. Chemical Geology, 81, 255–270.

Burnham, C.W. (1994) Development of the Burnham model for prediction of H_2O solubility in magmas. In Mineralogical Society of America Reviews in Mineralogy, 30, 123–129.

Clague, D.A., and Dalrymple, G.B. (1988) Age and petrology of alkalic postshield and rejuvenated stage lava from Kauai, Hawaii. Contributions to Mineralogy and Petrology, 99, 202–218.

Clague, D.A., and Frey, F.A. (1982) Petrology and trace element geochemistry of the Honolulu Volcanics, Implications for the oceanic mantle beneath Hawaii. Journal of Petrology, 23, 447–504.

Clague, D.A., Holcomb, R.T., Sinton, J.M., Detrick, R.S., and Torresan, M.R. (1990) Pliocene and Pleistocene alkalic flood basalts on the seafloor north of the Hawaiian islands. Earth and Planetary Science Letters, 98, 175–191.

Cocheo, P.A., and Holloway, J.R. (1993) The solubility of H_2O in basanitic melts at low pressures. EOS Transactions of the American Geophysical Union 74, Spring Meeting Supplemental, 350.

Dixon, J.E., and Pan, V. (1995) Determination of the molar absorptivity of dissolved carbonate in basanitic glass. American Mineralogist, 80, 1339–1342.

Dixon, J.E., and Stolper, E.M. (1995) An experimental study of H_2O and carbon dioxide solubilities in mid-ocean ridge basaltic liquids. Part II: Application to degassing of basaltic liquids. Journal of Petrology, 36, 1633–1646.

Dixon, J.E., Stolper, E.M., and Holloway, J.R. (1995) An experimental study of H_2O and carbon dioxide solubilities in mid-ocean ridge basaltic liquids. Part I: Calibration and solubility results. Journal of Petrology, 36, 1607–1631.

Dixon, J.E., Clague, D.A., Wallace, P., and Poreda, R. (1997) Volatiles in alkalic basalts from the North Arch Volcanic Field, Hawaii: Extensive degassing of deep submarine-erupted alkalic series lavas. Journal of Petrology, in press.

Eggler, D.H. (1974) Effect of CO_2 on the melting of peridotite. Carnegie Institute of Washington Yearbook, 72, 215–224.

Eitel, W., and Weyl, W. (1932) Residuals in the melting of commercial glasses. Journal of the American Ceramics Society, 15, 159–166.

Gerlach, T.M. (1986) Exsolution of H_2O, CO_2, and S during eruptive episodes at Kilauea Volcano, Hawaii. Journal of Geophysical Research, 91, 12177–12185.

Holloway, J.R. (1977) Fugacity and activity of molecular species in supercritical fluids. In Fraser, D., (Ed.), Thermodynamics in Geology, p. 161–181. Reidel, Boston.

Holloway, J.R., and Blank, J.G. (1994) Application of experimental results to C-O-H species in natural melts. In Mineralogical Society of America Reviews in Mineralogy, 30, 187–230.

Holloway, J.R., Mysen, B.O., and Eggler, D.H. (1976) The solubility of CO_2 in liquids on the join CaO-MgO-SiO_2-CO_2. Carnegie Institute of Washington Yearbook, 75, 626–631.

Jambon, A., Weber, H., and Braun, O. (1986) Solubility of He, Ne, Ar, Kr and Xe in a basalt melt in the range 1250–1600 °C. Geochemical implications. Geochimica et Cosmochimica Acta, 50, 401–408.

Mattey, D.P., Taylor, W.R., Green, D.H., and Pillinger, C.T. (1990) Carbon isotopic fractionation between CO2 vapour, silicate and carbonate melts: An experimental study to 30 kbar. Contributions to Mineralogy and Petrology, 104, 492–505.

McMillan, P. (1994) H_2O solubility and speciation models. In Mineralogical Society of America Reviews in Mineralogy, 30, 131–156.

McMillan, P., and Holloway, J.R. (1987) H_2O solubility in aluminosilicate melts. Contributions to Mineralogy and Petrology, 97, 320–332.

Mysen, B.O. (1976) The role of volatiles in silicate melts: Solubility of CO_2 and H_2O in feldspar, pyroxene, and feldspathoid melts to 30 kb and 1625 °C. American Journal of Science, 276, 969–996.

Mysen, B.O., Eggler, D.H., Setiz, M.G., Holloway, J.R. (1976) Carbon dioxide in silicate melts and crystals: Part I. Solubility measurements. American Journal of Science, 276, 455–579.

Moore, G.M., Vennemann, T., and Carmichael, I.S.E. (1995) Solubility of H_2O in magmas to 2 kbar. Geology, 23, 1099–1102.

Pan, V., Holloway, J.R., and Hervig, R.L. (1991) The pressure and temperature dependence of carbon dioxide solubility in tholeiitic basalt melts. Geochimica et Cosmochimica Acta, 55, 1587–1595.

Saxena, S.K., and Fei, Y. (1987) High pressure and high temperature fluid fugacities, Geochimica et Cosmochimica Acta, 51, 783–791.

Silver, L.A. and Stolper, E.M. (1989) H_2O in albitic glasses. Journal of Petrology, 30, 667–709.

Spera, F.J. and Bergman, S.C. (1980) Carbon dioxide in igneous petrogenesis: I. Contributions to Mineralogy and Petrology, 74, 55–66.

Thibault, Y., and Holloway, J.R. (1994) Solubility of CO_2 in a Ca-rich leucitite: Effects of pressure, temperature, and oxygen fugacity. Contributions to Mineralogy and Petrology, 116, 216–224, 1994.

Zhang, Y., and Zindler, A. (1989) Noble gas constraints on the evolution of the Earth's atmosphere. Journal of Geophysical Research, 94, 13719–13737.

Manuscript received February 2, 1996
Manuscript accepted December 11, 1996